

Understanding Prompt Tuning for V-L Models Through the Lens of Neural Collapse

Didi Zhu¹ Zexi Li¹ Min Zhang¹ Junkun Yuan¹,
Yunfeng Shao² Jiashuo Liu³ Kun Kuang¹ Yinchuan Li² Chao Wu¹

¹Zhejiang University ²Huawei Noah’s Ark Lab ³Tsinghua University

Abstract

Large-scale vision-language (V-L) models have demonstrated remarkable generalization capabilities for downstream tasks through prompt tuning. However, the mechanisms behind the learned text representations are unknown, limiting further generalization gains, especially under class imbalance scenarios. Recent advances in the neural collapse (NC) phenomenon of vision-only models suggest that the optimal representation structure is the simplex ETF, which paves the way to study representations in V-L models. In this paper, we make the first attempt to use NC for examining the representations in V-L models via prompt tuning. It is found that NC optimality of text-to-image representations shows a positive correlation with downstream generalizability, which is more severe under class imbalance settings. To improve the representations, we propose Neural-collapse-anchored Prompt Tuning (NPT), a novel method that learns prompts with text and image representations that satisfy the same simplex ETF. NPT incorporates two regularization terms: language-modality collapse and multi-modality isomorphism; and it is compatible with other prompt tuning methods. Extensive experiments show that NPT can consistently help to improve existing prompt tuning techniques across 11 datasets for both balanced and imbalanced settings.

1 Introduction

Recent advancements in the realm of large-scale vision-language (V-L) pre-trained models such as CLIP (Radford et al. 2021), have emerged as a promising alternative for visual representation learning. Drawing strength from millions of image-text pairs, these models proficiently align textual and visual modalities, showcasing promising performance on various downstream tasks such as zero-shot image recognition (Zhou et al. 2022b).

Despite these successes, emerging studies (Zhou et al. 2022a; Khattak et al. 2023) highlight the limitations of large V-L models in tasks where better generalization is needed, e.g., identifying novel classes. To mitigate these shortcomings without directly fine-tuning numerous parameters, many studies have devised methods for soft prompt tuning (Zhou et al. 2022a; Khattak et al. 2023). Soft prompt tuning enhances the generalization abilities of V-L models by freezing their core parameters and exclusively refining learnable prompts using a limited dataset. Building on CoOp (Zhou et al. 2022b) that models context words in prompts as learnable vectors, recent studies have introduced various techniques to enhance

the generalization by prompt tuning, including generating instance-specific prompt (Zhou et al. 2022a) and integrating additional vision-modality prompt (Khattak et al. 2023; Yao, Zhang, and Xu 2023).

The nature of prompt tuning is to learn text representations that are more adaptive to the image representations of the downstream tasks. Previous works attempted to hand-craft more effective prompt learning methods which seem to have better text representations, but they did not delve deeper into the mechanisms behind such representations. Therefore, in this paper, we wonder: (1) *What characterizes effective text and image representations in terms of V-L models’ generalizability?* (2) *How can we get those effective representations in the embedding space?*

An emerging discovery called neural collapse phenomenon (Papayan, Han, and Donoho 2020; Yang et al. 2022; Li et al. 2022) in the vision-only models has shed light on the optimal structure of visual feature representations. This phenomenon demonstrates that the last-layer features within the same class collapse to their within-class mean after the model reaches zero training loss on a sufficient and balanced dataset. Additionally, the within-class means and their corresponding classifier vectors converge to the vertices of a simplex equiangular tight frame (ETF). The simplex ETF depicts the geometric structure of several vectors that have maximal pairwise angles and equal norms (Papayan, Han, and Donoho 2020).

It inspires us to examine the text representation geometries in the prompt tuning of CLIP through the lens of neural collapse. After tuning prompts on a balanced dataset, text representations serve as classifier vectors and tend to approximate the ETF structure, as evident in Fig. 1 (a-b). Intuitively, the text representations of MaPLe are closer to the simplex ETF structure (i.e., with evenly maximal angles and equal norms) and are more aligned with the image representations than ZSCLIP, and MaPLe’s base-to-novel generalization is much better than ZSCLIP. We suppose that:

A better neural collapse phenomenon of text-to-image representations indicates better generalizability of prompt-tuned CLIP.

It is further validated by our empirical analysis in Fig. 2 (a). It is suggested that two metrics indicative of the ETF structure (further elaborated in Sec 4.1) exhibit a proportional correlation with CLIP’s base-to-novel generalization performances

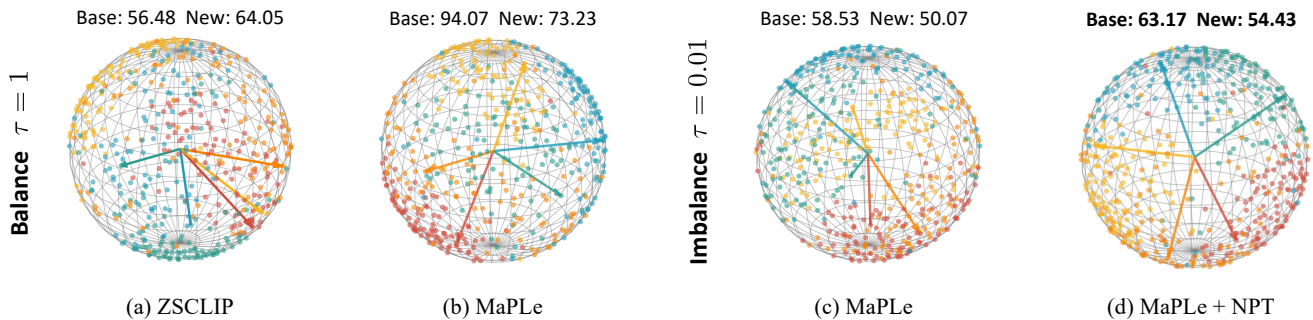


Figure 1: **Neural collapse degree visualization in CLIP on the EuroSAT dataset.** Arrows indicate text representations, points denote image representations, and colors indicate categories. (a-b) Under balanced conditions, the SOTA MaPLe method amplifies CLIP’s generalizability by intensifying the neural collapse degree. (c-d) Under imbalance, the optimal structure in MaPLe is disrupted, resulting in a performance drop. Our NPT method can refine this structure, improving generalization.

across several prompt tuning methods. Our analysis connects the text-to-image representations of CLIP with the neural collapse phenomenon and unveils the mechanism behind the good generalizability of prompt tuning.

Building on the findings, we further delve into a more practical setting where the downstream dataset is class imbalanced (Xie et al. 2023; ?). The class imbalance indicates that head classes contain most of the instances while tail classes have very few instances, which is prevalent in real-world scenarios. This imbalance can skew minor class representations and disturb the simplex ETF. As demonstrated in Fig. 1 (c), minor class text representations exhibit a tendency to cluster closely, a behavior that impairs the model’s capacity for generalization. This degradation of performance is further corroborated by the empirical evidence presented in Fig. 2 (b). To address the challenge, we propose a novel method called Neural-collapse-anchored Prompt Tuning (NPT), which aims to optimize prompts so that both text representations and image representations satisfy the same simplex ETF structure. Specifically, we introduce two regularization terms to the existing prompt tuning techniques. NPT considerably enhances the generalizability of V-L models in both class-imbalanced and balanced scenarios.

We summarize the contributions as follows:

- To the best of our knowledge, we are the first to extend the neural collapse phenomenon to V-L models and provide insights into the underlying representation mechanism of prompt tuning on CLIP’s generalization ability.
- We further explore the impact of class imbalance on the generalization performance of V-L models, addressing a critical gap in existing research. To mitigate this, we introduce NPT to improve CLIP’s generalization ability under both class balance and imbalance scenarios.
- Through theoretical analysis and extensive empirical experiments, we demonstrate the effectiveness of NPT combined with existing prompt tuning approaches, showcasing its significant improvements in generalization.

Our takeaway insights of the neural collapse are below:

- A higher degree of neural collapse in text-to-image representations is indicative of stronger generalizability. This

is pivotal in explaining how soft prompt tuning enhances CLIP’s generalization capability.

- Prompt tuning on an imbalanced dataset will disturb the text-to-image representations from neural collapse, thus, hurting the generalization. Neural-collapse-anchored approaches are needed to improve the representations.

2 Related Work

Vision-Language Models. The fusion of language supervision with natural images has garnered significant attention within the computer vision community. These V-L models, as opposed to those solely based on image supervision, encode rich language-driven visual multi-modal representations. Recent V-L models such as CLIP (Radford et al. 2021), ALIGN (Jia et al. 2021), LiT (Zhai et al. 2022), FILIP (Yao et al. 2021), and Florence (Yuan et al. 2021) have showcased remarkable performance across a diverse range of tasks, including few-shot and zero-shot visual recognition. These models learn joint image-language representations by self-supervised training on vast amounts of web data.

Prompt Learning. Prompt learning indicates that prompts can be learned automatically for a downstream task during the fine-tuning stage. This technique was first used in NLP (Li and Liang 2021; Lester, Al-Rfou, and Constant 2021; Liu et al. 2021) followed by the adaptation in V-L (Zhou et al. 2022b,a; Zhu et al. 2022). CoOp (Zhou et al. 2022b) fine-tunes CLIP for few-shot transfer learning by optimizing a continuous set of prompt vectors at its language branch. CoCoOp (Zhou et al. 2022a) highlights the inferior performance of CoOp on novel classes and solves the generalization issue by explicitly conditioning prompts on image instances. (Lu et al. 2022) proposes to optimize multiple sets of prompts by learning the distribution of prompts. (Bahng et al. 2022) perform visual prompt tuning on CLIP by prompting on the vision branch. MaPLe (Maaz et al. 2022) proposes multi-modal prompts in both language and vision branches of CLIP.

Neural Collapse. In (Papayan, Han, and Donoho 2020), neural collapse was observed that a linear classification model trained on a balanced dataset experiences a phenomenon where the last-layer features collapse into within-class centers during the final stage of training. Since then, researchers

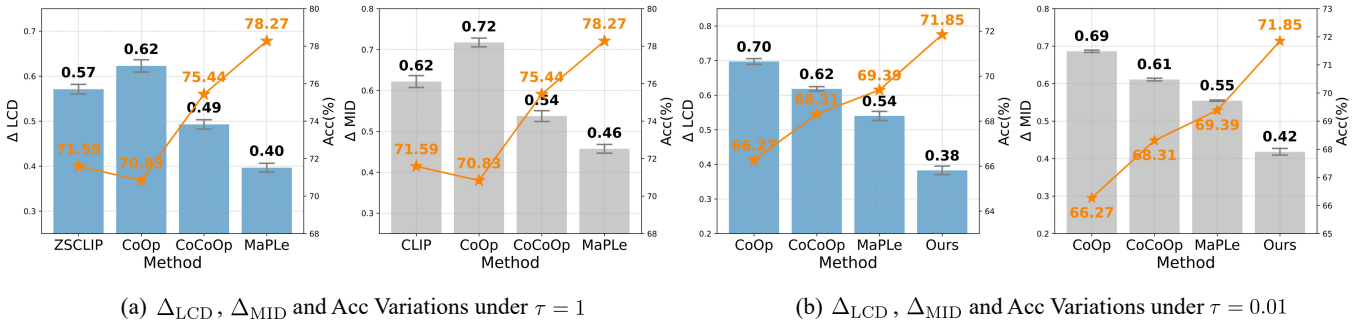


Figure 2: **Comparison of Δ_{MID} and Δ_{LCD} with generalization performance under the base-to-novel task.** τ denotes imbalance degree: $\tau = 1$ for balanced data and $\tau = 0.01$ for high imbalance. (a) In balanced settings, we compare Zero-shot CLIP with current soft prompt tuning methods, finding a direct correlation between Δ_{MID} & Δ_{LCD} errors (the smaller values, the greater neural collapse) and accuracy. (b) This correlation holds in class imbalance scenarios, where the degree of neural collapse and generalization performance are more impaired, even for the SOTA method MaPLE. Our approach effectively bolsters CLIP’s generalization in class imbalance settings by minimizing Δ_{LCD} and Δ_{MID} , thereby avoiding significant performance declines.

have endeavored to understand this phenomenon theoretically (Fang et al. 2021; Weinan and Wojtowytsch 2022; Ji et al. 2021; Zhu et al. 2021; Tirer and Bruna 2022). Recent studies have attempted to induce neural collapse in imbalanced learning (Yang et al. 2022; Xie et al. 2023; Thrapoulidis et al. 2022), incremental learning (Yang et al. 2023), semantic segmentation (Zhong et al. 2023), and federated learning (Li et al. 2023; Huang et al. 2023). However, these investigations into neural collapse are limited to linear classifiers. In this work, we explore the presence of such a solution in V-L models and propose NPT to improve the generalizability of V-L models through prompt tuning.

3 Preliminaries

3.1 Prompt Tuning in V-L models

CLIP comprises a vision-modality image encoder $G_v : \mathbb{R}^{w \times h \times 3} \rightarrow \mathbb{R}^d$ and a language-modality text encoder $G_l : \mathbb{R}^{m \times d_e} \rightarrow \mathbb{R}^d$. The image encoder G_v converts a 3-channel image \mathbf{x} with shape $w \times h$ into a d -dimensional image representation $\mathbf{z} \in \mathbb{R}^d$. Meanwhile, the text encoder G_l generates a d -dimensional text representation $\mathbf{g}_k \in \mathbb{R}^d$ from m -words d_e -dimensional text input \mathbf{t}_k , where $k \in \{1, \dots, K\}$ and K is the number of classes. Note that both \mathbf{z} and \mathbf{g}_k are ℓ_2 normalized vectors. Two encoders are jointly trained using a contrastive loss that maximizes the cosine similarity of matched pairs and minimizes that of the unmatched pairs.

Prompt engineering adapts the pre-trained CLIP to perform zero-shot recognition without fine-tuning the model. Denote $\mathbb{V} = \{\text{class}_k\}_{k=1}^K$ as a class name set, the text input for CLIP is obtained by extending $[\text{class}_k]$ using a template like $\mathbf{t}_k = \text{"a photo of a } [\text{class}_k] \text{"}$. The corresponding text representation \mathbf{g}_k is obtained by feeding the prompt into the text encoder G_l , while the image representation \mathbf{z} of the image \mathbf{x} is extracted by the image encoder G_v .

Soft prompt learning replaces the hand-crafted prompts with learnable prompts. CoOp (Zhou et al. 2022b) and CoCoOp (Zhou et al. 2022a) incorporate b learnable tokens $\{\mathbf{u}_1, \dots, \mathbf{u}_b\}$ for modeling text prompts, whereas MaPLE (Maaz et al. 2022) extends the approach by introducing an

additional set of b learnable tokens $\{\mathbf{v}_1, \dots, \mathbf{v}_b\}$ to model vision prompts. Denote c_k as the word embedding of the k -th class name, the text prompt of k -th class is formulated as $\mathbf{t}_k = \{\mathbf{u}_1, \dots, \mathbf{u}_b, c_k\}$. For an image \mathbf{x} , its visual prompt is represented as $\mathbf{f} = \{\mathbf{v}_1, \dots, \mathbf{v}_b, \mathbf{x}\}$. Therefore, the probability that \mathbf{x} belongs to the k -th class can be expressed as:

$$p_{\text{soft}}(y = k | \mathbf{x}) = \frac{\exp(\langle G_v(\mathbf{f}), G_l(\mathbf{t}_k) \rangle / \lambda)}{\sum_{i=1}^K \exp(\langle G_v(\mathbf{f}), G_l(\mathbf{t}_i) \rangle / \lambda)}. \quad (1)$$

Note that the prediction probability can be represented by replacing $G_v(\mathbf{f})$ with $G_v(\mathbf{x}) = \mathbf{z}$ in hand-crafted prompt engineering and vision-only prompt tuning.

3.2 Neural Collapse in Linear Classifier

Neural collapse describes that, at the terminal training phase, the within-class means together with the linear classifier vectors will collapse to the vertices of a simplex equiangular tight frame (ETF), which is defined as follows.

Definition 1 (Simplex Equiangular Tight Frame). *Consider a set of vectors $\mathbf{m}_i \in \mathbb{R}^d$, with $i = 1, \dots, K$, and $d \geq K - 1$. This collection of vectors forms a simplex equiangular tight frame if:*

$$\mathbf{M} = \sqrt{\frac{K}{K-1}} \mathbf{u} \left(\mathbf{I}_K - \frac{1}{K} \mathbf{1}_K \mathbf{1}_K^T \right), \quad (2)$$

where $\mathbf{M} = [\mathbf{m}_1, \dots, \mathbf{m}_K] \in \mathbb{R}^{d \times K}$, $\mathbf{u} \in \mathbb{R}^{d \times K}$ allows a rotation and satisfies $\mathbf{u}^T \mathbf{u} = \mathbf{I}_K$, \mathbf{I}_K is the identity matrix, and $\mathbf{1}_K$ is an all-ones vector. All vectors in a simplex ETF have an equal ℓ_2 norm and the same pair-wise angle, i.e.,

$$\mathbf{m}_i^T \mathbf{m}_j = \frac{K}{K-1} \delta_{i,j} - \frac{1}{K-1}, \forall i, j \in [K], \quad (3)$$

where $\delta_{i,j}$ equals to 1 when $i = j$ and 0 otherwise. The pair-wise angle $-\frac{1}{K-1}$ is the maximal equiangular separation of K vectors in \mathbb{R}^d (Pappayan, Han, and Donoho 2020).

Denote $\mathbf{z}_{k,i}$ as the last-layer image representation of the i -th sample in the k -th class, the prototype $\mathbf{z}_k = \text{Avg}_i\{\mathbf{z}_{k,i}\}$

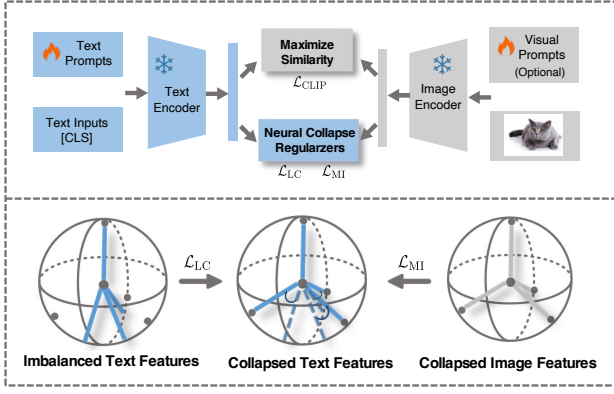


Figure 3: **Overview of Neural-collapse-anchored Prompt Tuning (NPT).** Our method capitalizes on the benefits of two distinct regularizers: LC Regularizer \mathcal{L}_{LC} , which controls the increase in Δ_{LCD} values and fosters the generation of more discriminative textual representations; and MI Regularizer \mathcal{L}_{MI} , which promotes enhanced multi-modal alignment to address challenges and attain a reduced Δ_{MID} .

is the mean value of the features in the k -th class, w_k is the classifier vector of the k -th class. We define three properties instructed by neural collapse in vision-only models below:

Feature Collapse: For any $k \in \{1, \dots, K\}$, the last-layer features in the k -th class collapse to their prototype, i.e., the k -th within-class covariance $\Sigma_k \rightarrow \mathbf{0}$, where $\Sigma_k := \text{Avg}_{k,i} \left\{ (\mathbf{z}_{k,i} - \mathbf{z}_k)(\mathbf{z}_{k,i} - \mathbf{z}_k)^T \right\}$ and $\text{Avg}\{\cdot\}$ indicates the average operation.

Prototype Collapse: For any $k \in \{1, \dots, K\}$, the normalized prototypes converge to a simplex ETF, i.e., $\tilde{\mathbf{z}}_k = (\mathbf{z}_k - \mathbf{z}_G) / \|\mathbf{z}_k - \mathbf{z}_G\|$, satisfies Eq. 3, where \mathbf{z}_G is the global mean of the last-layer features, i.e., $\mathbf{z}_G = \text{Avg}_{k,i} \{ \mathbf{z}_{k,i} \}$.

Classifier Collapse: For any $k \in \{1, \dots, K\}$, the normalized classifier vectors converge to the same simplex ETF as prototypes, i.e., $\tilde{\mathbf{w}}_k = \mathbf{w}_k / \|\mathbf{w}_k\| = \mathbf{z}_k$, satisfies Eq. 3.

4 Method

4.1 Explore Neural Collapse in CLIP

The intriguing neural collapse (NC) phenomenon has primarily been observed and examined in vision-only models. In this paper, we investigate the corresponding structures in the vision-language model CLIP, a model that performs recognition by evaluating similarities between text and image representations. In consideration of the multi-modality aspect of the V-L model, we design two evaluation criteria during training to assess the presence of neural collapse phenomena in the V-L model. The definitions are as follows:

Definition 2 (Language-modality Collapse Degree). *Given a text encoder $G_l(\cdot)$, the language-modality collapse degree (LCD) of text representations is given by*

$$\Delta_{LCD} = \text{Avg}_{i \neq j} \left\{ \langle G_l(\mathbf{t}_i), G_l(\mathbf{t}_j) \rangle - E_W \cdot \mu \right\},$$

$$\text{s.t. } \|G_l(\mathbf{t}_i)\|^2 \leq E_W, \forall 1 \leq i \leq K,$$

where $\mu = -\frac{1}{K-1}$, $\mathbf{t}_i, \mathbf{t}_j$ are text prompts of $G_l(\cdot)$ and $\sqrt{E_W}$ is the fixed length constraint for text representations.

Definition 3 (Multi-modality Isomorphism Degree). *Given a text encoder $G_l(\cdot)$ and an image encoder $G_v(\cdot)$, the multi-modality isomorphism degree (MID) is given by*

$$\Delta_{MID} = \text{Avg}_{k,i} \left\{ \langle G_v(\mathbf{f}_{k,i}), G_l(\mathbf{t}_k) \rangle - \sqrt{E_W \cdot E_H} \right\},$$

$$\text{s.t. } \|G_l(\mathbf{t}_i)\|^2 \leq E_W, \forall 1 \leq i \leq K,$$

$$\|G_v(\mathbf{f}_{k,i})\|^2 \leq E_H, \forall 1 \leq k \leq K, 1 \leq i \leq n_k,$$

where $\mathbf{f}_{k,i}$ is the image input of \mathbf{x}_i in the k -th class and n_k is the number of samples belonging to the k -th class. $\sqrt{E_H}$ is the fixed length constraint for image features.

Remark 1. Δ_{LCD} measures the degree of separation among text representations (equivalent to classification vectors in vision-only models), reflecting the proximity between the language-modality structure and the simplex ETF. Δ_{MID} characterizes the discrepancy between the image representation and its text representation, reflecting the alignment degree of language- and vision-modality structure. Lower Δ_{LCD} and Δ_{MID} indicate that text representations and image representations are more aligned and closer to the same simplex ETF.

As illustrated in Fig. 2, we analyzed the variations in Δ_{LCD} and Δ_{MID} values across different class distributions on the base-to-novel task. The reported values represent the average across 11 datasets. Furthermore, we visualize the neural collapse degree for the novel classes on the EuroSAT dataset, as depicted in Fig. 1. Under balanced training data conditions, the current SOTA prompt tuning method MaPLe exhibits relatively low Δ_{LCD} and Δ_{MID} values compared with ZSCLIP and other methods. This suggests a clear correlation between these values and model accuracy. However, when encountering imbalanced training data, an observable increase in both values is detected, leading to a subsequent decline in accuracy. We can deduce that: (1) a higher degree of neural collapse, i.e., smaller values of Δ_{LCD} and Δ_{MID} , leads to stronger generalizability, and (2) data imbalance during training disrupts the neural collapse degree, subsequently affecting generalization performance. These observations can be explicitly represented as:

$$\tau \uparrow \implies \Delta_{LCD} \uparrow, \Delta_{MID} \uparrow \implies \text{Acc} \downarrow \quad (4)$$

Based on these observations, we propose the Neural-collapse-anchored Prompt Tuning (NPT) method, which optimizes the prompt by introducing two regularizers to implicitly address the drop in these values even under class imbalance. As illustrated in Fig. 1 (d) and Fig. 2 (b), our NPT enables multi-modality structures to approach the simplex ETF, thereby improving CLIP’s generalization performance.

4.2 Neural-collapse-anchored Prompt Tuning

In this subsection, we propose two neural-collapse-anchored regularization terms: Language-modality Collapse (LC) Regularizer and Multi-modality Isomorphism Degree (MI) Regularizer, which are guided by Δ_{LCD} and Δ_{MID} respectively.

Language-modality Collapse Regularization is introduced to address the issue in language-modality where certain text

representations are situated exceptionally close while others remain distantly apart. Achieving an equitable and maximal separation among text representations is the key to the generalizability of CLIP. Hence, the LC regularizer encourages the similarity between any two text representations from different classes to approach μ (specified in Definition 1):

$$\mathcal{L}_{\text{LC}} = \sum_{i=1}^K \sum_{j=1, i \neq j}^K (\langle G_l(\mathbf{t}_i), G_l(\mathbf{t}_j) \rangle - E_W \cdot \mu)^2. \quad (5)$$

where $\|G_l(\mathbf{t}_i)\|^2 \leq E_W$, $i = 1, \dots, K$. E_W is the class-wise constraints for text representation $G_l(\mathbf{t}_i)$.

Multi-modality Isomorphism Regularization aims to tackle the issue of multi-modality isomorphism degree (MID) by optimizing the alignment between language and visual modalities as follows:

$$\mathcal{L}_{\text{MI}} = \sum_{k=1}^K \sum_{i=1}^{n_k} (\langle G_v(\mathbf{f}_{k,i}), G_l(\mathbf{t}_k) \rangle - \sqrt{E_W \cdot E_H})^2, \quad (6)$$

where $\|G_v(\mathbf{f}_{k,i})\|^2 \leq E_H$, $i = 1, \dots, K$. E_H is the instance-wise constraints for image representation $G_v(\mathbf{f}_{k,i})$. By minimizing the MI loss term, our goal is to foster strong alignment between language and visual representations, which in turn improves model performance when handling diverse and imbalanced data distributions.

Overall Framework. By incorporating our proposed regularization terms into the contrastive loss function within the current prompt learning techniques, we can optimize the prompts effectively using the overall loss:

$$\mathcal{L} = \mathcal{L}_{\text{CLIP}} + w_1 \mathcal{L}_{\text{LC}} + w_2 \mathcal{L}_{\text{MI}} \quad (7)$$

where $\mathcal{L}_{\text{CLIP}} = -\frac{1}{N} \sum_{\mathbf{x} \in \mathcal{X}} \sum_{k=1}^K y_{\mathbf{x},k} p_{\text{soft}}(y = k | \mathbf{x})$, w_1 and w_2 are hyperparameters governing the contribution of each component.

As illustrated in Fig. 3, the proposed approach harnesses the strengths of both regularizers: LC Regularizer for minimizing Δ_{LCD} value and developing more discriminative text representations, and MI Regularizer for facilitating better multi-modality alignment to achieve a lower Δ_{MID} .

4.3 Theoretical Analysis

Gradient w.r.t. text prompt under class imbalance. We first analyze the gradient of $\mathcal{L}_{\text{CLIP}}$ w.r.t text representations:

$$\frac{\partial \mathcal{L}_{\text{CLIP}}}{\partial G_l(\mathbf{t}_k)} = \underbrace{\sum_{i=1}^{n_k} (p_k(\mathbf{z}_{k,i}) - 1) \mathbf{z}_{k,i}}_{\text{intra-class cohesion}} + \underbrace{\sum_{k' \neq k} \sum_{j=1}^{n_{k'}} p_{k'}(\mathbf{z}_{k',j}) \mathbf{z}_{k',j}}_{\text{inter-class repulsion}}$$

where $\mathbf{z}_{k,i} = G_v(\mathbf{f}_{k,i})$, $p_k(\mathbf{z}_{k,i}) = p_{\text{soft}}(y = k | \mathbf{x}_{k,i})$ is the predicted probability that $\mathbf{z}_{k,i}$ belongs to the k -th class.

Remark 2. The gradient equation is composed of two terms. The "intra-class cohesion" term comprises n_k elements, directs $G_l(\mathbf{t}_k)$ towards its corresponding image representations $\mathbf{z}_{k,i}$. In contrast, the "inter-class repulsion" term, with $N - n_k$ elements, pushes $G_l(\mathbf{t}_k)$ against features of other classes. Consequently, gradients of certain minor classes are overwhelmingly influenced by the repulsion term due to the small n_k and large $N - n_k$.

To tackle this issue, we introduce \mathcal{L}_{LC} . The corresponding gradient equation w.r.t. \mathbf{t}_i is defined as:

$$\frac{\partial \mathcal{L}_{\text{LC}}}{\partial \mathbf{t}_i} = \sum_{j=1, i \neq j}^K 2 (S_{ij} - E_W \cdot \mu) \left\langle \frac{\partial G_l(\mathbf{t}_i)}{\partial \mathbf{t}_i}, G_l(\mathbf{t}_j) \right\rangle,$$

where $S_{ij} = \langle G_l(\mathbf{t}_i), G_l(\mathbf{t}_j) \rangle$, $S'_{ik} = \langle G_v(\mathbf{f}_{k,i}), G_l(\mathbf{t}_k) \rangle$. \mathcal{L}_{LC} can explicitly adjust the prompt \mathbf{t}_i to ensure text representations are maximally angularly separated, i.e., $S_{ij} - E_W \cdot \mu$. This regularizer effectively mitigates the adverse effects of imbalanced gradient updates in $\mathcal{L}_{\text{CLIP}}$.

Gradient w.r.t. image prompt. The gradient of $\mathcal{L}_{\text{CLIP}}$ with respect to the image representation \mathbf{z}_i is:

$$\frac{\partial \mathcal{L}_{\text{CLIP}}}{\partial G_v(\mathbf{f}_i)} = (p_k(\mathbf{z}_{k,i}) - 1) G_l(\mathbf{t}_k) + \sum_{k' \neq k} p_{k'}(\mathbf{z}_{k',i}) G_l(\mathbf{t}_{k'}).$$

where $\mathbf{z}_{k,i} = G_v(\mathbf{f}_{k,i})$, k is the class label of $\mathbf{z}_{k,i}$.

Remark 3. This gradient formula is similar to $\frac{\partial \mathcal{L}_{\text{CLIP}}}{\partial G_l(\mathbf{t}_k)}$. It aims to bring image representations closer to text representations of the same class and farther away from those of other classes. However, text representations can be influenced by imbalance, causing the representations of minor classes to be close together. Optimizing image representations towards biased text representations can compromise performance.

Similarly, we analyze the gradient of \mathcal{L}_{MI} w.r.t. $\mathbf{f}_{k,i}$:

$$\frac{\partial \mathcal{L}_{\text{MI}}}{\partial \mathbf{f}_{k,i}} = 2 \left(S'_{ik} - \sqrt{E_W E_H} \right) \left\langle \frac{\partial G_v(\mathbf{f}_{k,i})}{\partial \mathbf{f}_{k,i}}, G_l(\mathbf{t}_k) \right\rangle.$$

\mathcal{L}_{MI} ensures that image representations closely align with text representations of the same class, uninfluenced by imbalances, as represented by $S'_{ik} - \sqrt{E_W E_H}$. This bolsters the discriminative power, especially for minor classes.

5 Experiment

Our approach is evaluated on (1) base-to-novel class identification, (2) cross-dataset transfer, and (3) domain generalization, under three class imbalance degrees. All trained data are created by downsampling each class's samples to obey an exponential decay with three imbalance ratios $\tau = \{1, 0.05, 0.01\}$. Here $\tau = \min\{n_k\} / \max\{n_k\}$ with n_k being the number of samples in the k -th class and $\max\{n_k\} = 16$.

Datasets. For the first two settings, i.e., base-to-novel generalization and cross-dataset transfer, we use the 11 image recognition datasets as in (Zhou et al. 2022b,a). For domain generalization experiments, we use ImageNet as the source dataset and four other variants of ImageNet that contain different types of domain shifts as the target dataset, following (Zhou et al. 2022a). See more details in the Appendix.

Implementation Details. Since our method is orthogonal to the other prompt tuning methods, we combine NPT with the existing CoCoOp and MaPLe, to demonstrate its flexibility and effectiveness. We apply prompt tuning on ViT-B/16 CLIP where $d = 512$. All models are trained for 5 epochs with a batch size of 4 and a learning rate of 0.0035 via SGD optimizer. Both E_W and E_H are set at 1, while w_1 and w_2 are assigned as 0.3 and 0.8, respectively. We follow other default hyperparameters used in MaPLe (Maaz et al. 2022).

Table 1: Harmonic mean values (%) on 11 datasets with different imbalance ratios on the base-to-novel task.

Method	Balance with $\tau = 1$											
	IN.	Cal.	OP.	SC.	Flw.	Food.	FA.	SUN.	DTD	ES.	UCF.	Avg
CLIP	70.22	95.40	94.12	68.65	74.83	90.66	31.09	72.23	56.37	60.03	73.85	71.58
CoCoOp	73.10	95.84	96.43	72.01	81.71	90.99	27.74	78.27	64.85	71.21	77.64	75.44
MaPLE	73.47	96.02	96.58	73.47	82.56	91.38	36.50	79.75	68.16	82.35	80.77	78.27
CoCoOp + NPT	73.78	97.05	96.88	72.50	83.01	91.20	35.03	78.67	66.88	74.52	78.82	77.12
MaPLE + NPT	74.02	96.46	96.54	72.71	82.94	91.75	35.54	79.88	69.20	82.85	81.42	78.48

Method	Imbalance Ratio $\tau = 0.05$											
	IN.	Cal.	OP.	SC.	Flw.	Food.	FA.	SUN.	DTD	ES.	UCF.	Avg
CoCoOp	70.34	95.29	95.11	69.48	75.03	89.61	21.78	74.67	57.94	62.33	72.83	71.31
MaPLE	70.93	95.38	94.22	70.25	76.59	88.71	28.62	75.98	55.15	51.10	75.43	71.12
CoCoOp + NPT	71.21	95.95	95.97	70.69	75.72	90.13	23.28	75.67	59.69	63.78	74.33	72.40
MaPLE + NPT	72.28	95.82	96.31	71.07	78.76	90.47	30.24	76.94	57.35	58.14	76.65	73.09

Method	Imbalance Ratio $\tau = 0.01$											
	IN.	Cal.	OP.	SC.	Flw.	Food.	FA.	SUN.	DTD	ES.	UCF.	Avg
CoCoOp	68.88	94.54	94.71	68.45	71.24	88.31	11.48	73.87	52.39	57.45	70.11	68.31
MaPLE	70.10	95.53	94.21	69.29	72.29	89.74	21.89	75.00	47.37	53.97	73.85	69.38
CoCoOp + NPT	70.23	95.16	95.66	70.17	73.50	90.08	20.34	74.42	54.97	62.95	71.01	70.77
MaPLE + NPT	70.89	95.64	94.56	70.58	74.46	90.20	27.72	75.89	56.98	58.48	74.95	71.85

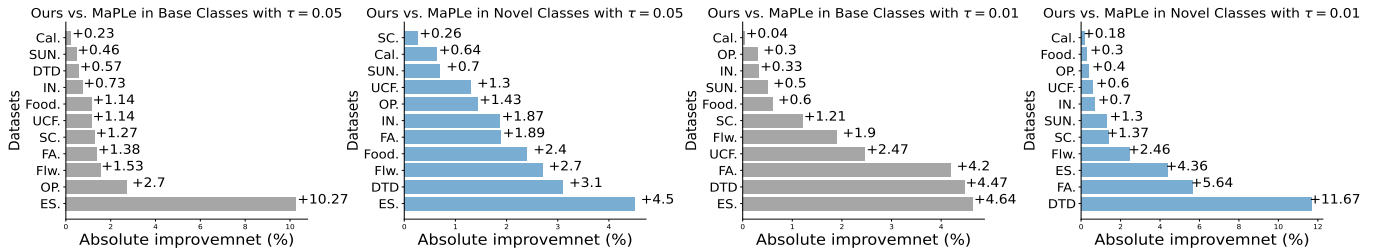


Figure 4: Absolute improvement of NPT over MaPLE in the base-to-novel generalization task. Compared with MaPLE, our method achieves improvement for both base and new classes on all datasets with $\tau = 0.05$ and $\tau = 0.01$.

5.1 Base-to-Novel Generalization

Following the previous works (Zhou et al. 2022a; Khattak et al. 2023), for each dataset, we split the classes equally into two groups: the base classes and the novel classes. The learnable modules are trained exclusively on the imbalanced base classes, while evaluation is carried out separately on both the base and novel classes to testify to generalization ability. Table 1 presents the harmonic mean values for 11 datasets on the base-to-novel tasks. Detailed base and novel accuracy figures can be found in the Appendix. When trained on imbalanced base classes, both CoCoOp and MaPLE see performance dips of 4.13% and 7.15% respectively at $\tau = 0.05$, and 7.13% and 8.89% at $\tau = 0.01$, underscoring the catastrophic impact of class imbalance on generalization. Our method exhibits improvements of 1.97% when $\tau = 0.05$, and improvements of 2.47% when $\tau = 0.01$ over MaPLE.

We further compare the accuracy gains of MaPLE on both novel and base classes before and after integrating NPT in Fig. 4. Our method significantly outperforms MaPLE in both base and novel classes across all 11 datasets. Interestingly, we observe that NPT offers a more substantial improvement in recognizing novel classes, highlighting its potential in

challenging generalization scenarios.

5.2 Cross-Dataset Transfer

We then evaluate the generalization ability of our method on more challenging cross-dataset tasks. In this setting, we learn prompts on ImageNet of 1000 classes with three different imbalance ratios. The effectiveness of the learned prompts is then tested on the other 10 datasets. The results are reported in Table 2. The same performance drop phenomenon can be observed in cross-dataset tasks due to data imbalance, and combining NPT with CoCoOp and MaPLE can improve this drop. MaPLE+NPT achieves the best results at all imbalance ratios, demonstrating the great transfer ability of our method.

5.3 Domain Generalization

We perform experiments with ImageNet as the source domain and evaluate its ability to generalize to four distinct ImageNet variants, which serve as unseen target domains. Table 4 presents the results, indicating that our method significantly improves the performance on the four ImageNet variants with two imbalance ratios. This confirms that our approach enhances the discriminability of the source dataset

Table 2: Comparison of NPT with existing approaches on cross-dataset task.

	Imbalance Ratio $\tau = 0.05$											
	IN. \rightarrow	Cal.	OP.	SC.	Flw.	Food.	FA.	SUN.	DTD	ES.	UCF.	Avg
CoCoOp	69.93	93.18	89.88	65.09	71.02	85.21	20.02	66.89	44.25	44.34	66.53	64.64
MaPLe	69.20	92.23	90.34	65.17	71.54	85.03	21.39	65.57	45.84	47.83	65.34	65.03
CoCoOp + NPT	70.14	93.52	91.56	66.43	71.43	85.98	22.34	67.42	45.33	44.90	67.24	65.62
MaPLe + NPT	69.40	93.31	90.64	65.95	72.62	86.19	22.78	66.89	46.05	50.25	67.12	66.18

	Imbalance Ratio $\tau = 0.01$											
	IN. \rightarrow	Cal.	OP.	SC.	Flw.	Food.	FA.	SUN.	DTD	ES.	UCF.	Avg
CoCoOp	68.42	92.45	89.21	64.34	70.32	84.13	19.88	65.07	44.09	44.18	64.31	63.80
MaPLe	68.32	92.63	90.07	64.38	70.37	84.77	20.47	64.53	45.17	47.03	64.40	64.38
CoCoOp + NPT	68.88	93.03	90.12	65.22	70.88	85.65	20.87	66.23	45.34	44.89	65.91	64.81
MaPLe + NPT	68.90	93.60	89.93	65.28	71.77	86.21	21.51	66.07	44.97	49.67	66.20	65.52

Table 3: Ablation study of each loss module in NPT on three generalization tasks with $\tau = 0.01$.

	Base-to-Novel	Cross-Dataset	Domain Generalization
MaPLe	69.38	63.99	59.12
+ \mathcal{L}_{LC}	70.02	64.01	59.45
+ \mathcal{L}_{MI}	70.43	64.32	59.48
+ NPT	71.85	64.89	59.53

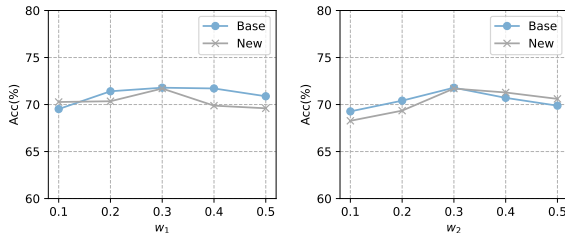


Figure 5: Sensitivity analysis of w_1 and w_2 under base-to-novel task with $\tau = 0.01$.

while preserving its generalization to the target domain.

5.4 Improvement of NPT on Balanced Datasets

In Table 1, we showcase the improvement of NPT on balanced datasets under the base-to-novel task. Our NPT can improve generalization for most of the datasets (9/11), and the maximal performance gain is up to 1.3%. Due to space constraints, other experimental results with balanced data ($\tau = 1$) regarding cross-dataset transfer and domain generalization are provided in the Appendix.

5.5 Ablation Study

Effectiveness of each module. We conduct ablation experiments on three tasks to assess the effectiveness of the \mathcal{L}_{LCD} and \mathcal{L}_{MID} of NPT, as presented in Table 3. The results demonstrate that each module has a significant positive impact on the model’s performance. Specifically, for the base-to-novel task, the \mathcal{L}_{LCD} and \mathcal{L}_{MID} modules improve the results by 0.64% and 1.05%, respectively. Furthermore, the combination of these modules leads to a remarkable improvement

Table 4: Comparison of NPT with existing approaches on domain generalization task.

	Imbalance Ratio $\tau = 0.05$					
	IN. \rightarrow	IN.-V2	IN.-S	IN.-A	IN.-R	Avg
CoCoOp	68.43	62.21	46.89	48.56	75.64	60.37
MaPLe	69.20	62.40	48.27	50.98	76.83	59.62
CoCoOp+NPT	69.65	64.32	47.41	48.99	77.89	61.65
MaPLe+NPT	69.40	63.10	48.83	51.10	77.20	60.06

	Imbalance Ratio $\tau = 0.01$					
	IN. \rightarrow	IN.-V2	IN.-S	IN.-A	IN.-R	Avg
CoCoOp	66.21	60.35	46.13	50.25	74.56	57.82
MaPLe	67.32	62.33	47.20	50.47	76.47	59.12
CoCoOp+NPT	67.57	62.04	47.55	50.38	75.88	58.96
MaPLe+NPT	68.70	62.83	48.53	50.07	76.70	59.53

of 2.47%. These findings suggest that both modules play a crucial role in enhancing the model’s generalization ability. **Sensitivity Analysis of w_1 and w_2 .** In Fig. 3, we analyze the impact of the hyperparameters w_1 and w_2 of Eq. 7. The results show that our method’s performance remains relatively stable across a broad range of w_1 and w_2 values, indicating the robustness of our approach to these hyperparameters. This suggests that our method can be effectively applied to a variety of downstream tasks with different parameter settings.

6 Conclusions

In this paper, we explore the text-to-image representation geometry of CLIP prompt tuning from the perspective of neural collapse. It is found that class imbalance has detrimental effects on representation, thus hurting generalization. We propose Neural-collapse-anchored Prompt Tuning (NPT), a method that optimizes prompts to ensure text and image representations share the same simplex ETF structure. By incorporating language-modality collapse and multi-modality isomorphism regularization terms, NPT enhances V-L models’ generalizability. Experiments show that NPT outperforms existing techniques across 11 diverse datasets under base-to-novel, cross-dataset, and domain generalization tasks.

References

- Bahng, H.; Jahanian, A.; Sankaranarayanan, S.; and Isola, P. 2022. Visual Prompting: Modifying Pixel Space to Adapt Pre-trained Models. *arXiv preprint arXiv:2203.17274*.
- Fang, C.; He, H.; Long, Q.; and Su, W. J. 2021. Exploring deep neural networks via layer-peeled model: Minority collapse in imbalanced training. *Proceedings of the National Academy of Sciences*, 118(43): e2103091118.
- Huang, C.; Xie, L.; Yang, Y.; Wang, W.; Lin, B.; and Cai, D. 2023. Neural Collapse Inspired Federated Learning with Non-iid Data. *arXiv preprint arXiv:2303.16066*.
- Ji, W.; Lu, Y.; Zhang, Y.; Deng, Z.; and Su, W. J. 2021. An unconstrained layer-peeled perspective on neural collapse. *arXiv preprint arXiv:2110.02796*.
- Jia, C.; Yang, Y.; Xia, Y.; Chen, Y.-T.; Parekh, Z.; Pham, H.; Le, Q.; Sung, Y.-H.; Li, Z.; and Duerig, T. 2021. Scaling up visual and vision-language representation learning with noisy text supervision. 4904–4916. PMLR.
- Khattak, M. U.; Rasheed, H.; Maaz, M.; Khan, S.; and Khan, F. S. 2023. Maple: Multi-modal prompt learning. In *Proceedings of the IEEE/CVF Conference on Computer Vision and Pattern Recognition*, 19113–19122.
- Lester, B.; Al-Rfou, R.; and Constant, N. 2021. The power of scale for parameter-efficient prompt tuning.
- Li, X.; Liu, S.; Zhou, J.; Lu, X.; Fernandez-Granda, C.; Zhu, Z.; and Qu, Q. 2022. Principled and Efficient Transfer Learning of Deep Models via Neural Collapse. *arXiv preprint arXiv:2212.12206*.
- Li, X. L.; and Liang, P. 2021. Prefix-tuning: Optimizing continuous prompts for generation.
- Li, Z.; Shang, X.; He, R.; Lin, T.; and Wu, C. 2023. No Fear of Classifier Biases: Neural Collapse Inspired Federated Learning with Synthetic and Fixed Classifier. *arXiv preprint arXiv:2303.10058*.
- Liu, X.; Ji, K.; Fu, Y.; Du, Z.; Yang, Z.; and Tang, J. 2021. P-tuning v2: Prompt tuning can be comparable to fine-tuning universally across scales and tasks.
- Lu, Y.; Liu, J.; Zhang, Y.; Liu, Y.; and Tian, X. 2022. Prompt Distribution Learning. 5206–5215.
- Maaz, M.; Rasheed, H.; Khan, S.; Khan, F. S.; Anwer, R. M.; and Yang, M.-H. 2022. Class-agnostic Object Detection with Multi-modal Transformer. Springer.
- Papayan, V.; Han, X.; and Donoho, D. L. 2020. Prevalence of neural collapse during the terminal phase of deep learning training. *Proceedings of the National Academy of Sciences*, 117(40): 24652–24663.
- Radford, A.; Kim, J. W.; Hallacy, C.; Ramesh, A.; Goh, G.; Agarwal, S.; Sastry, G.; Askell, A.; Mishkin, P.; Clark, J.; et al. 2021. Learning transferable visual models from natural language supervision. 8748–8763. PMLR.
- Thrapoulidis, C.; Kini, G. R.; Vakilian, V.; and Behnia, T. 2022. Imbalance trouble: Revisiting neural-collapse geometry. *Advances in Neural Information Processing Systems*, 35: 27225–27238.
- Tirer, T.; and Bruna, J. 2022. Extended unconstrained features model for exploring deep neural collapse. In *International Conference on Machine Learning*, 21478–21505. PMLR.
- Weinan, E.; and Wojtowytsch, S. 2022. On the emergence of simplex symmetry in the final and penultimate layers of neural network classifiers. In *Mathematical and Scientific Machine Learning*, 270–290. PMLR.
- Xie, L.; Yang, Y.; Cai, D.; and He, X. 2023. Neural collapse inspired attraction-repulsion-balanced loss for imbalanced learning. *Neurocomputing*.
- Yang, Y.; Xie, L.; Chen, S.; Li, X.; Lin, Z.; and Tao, D. 2022. Do we really need a learnable classifier at the end of deep neural network? *arXiv preprint arXiv:2203.09081*.
- Yang, Y.; Yuan, H.; Li, X.; Lin, Z.; Torr, P.; and Tao, D. 2023. Neural collapse inspired feature-classifier alignment for few-shot class incremental learning. *arXiv preprint arXiv:2302.03004*.
- Yao, H.; Zhang, R.; and Xu, C. 2023. Visual-language prompt tuning with knowledge-guided context optimization. In *Proceedings of the IEEE/CVF Conference on Computer Vision and Pattern Recognition*, 6757–6767.
- Yao, L.; Huang, R.; Hou, L.; Lu, G.; Niu, M.; Xu, H.; Liang, X.; Li, Z.; Jiang, X.; and Xu, C. 2021. Filip: Fine-grained interactive language-image pre-training. *arXiv preprint arXiv:2111.07783*.
- Yuan, L.; Chen, D.; Chen, Y.-L.; Codella, N.; Dai, X.; Gao, J.; Hu, H.; Huang, X.; Li, B.; Li, C.; et al. 2021. Florence: A new foundation model for computer vision. *arXiv preprint arXiv:2111.11432*.
- Zhai, X.; Wang, X.; Mustafa, B.; Steiner, A.; Keysers, D.; Kolesnikov, A.; and Beyer, L. 2022. Lit: Zero-shot transfer with locked-image text tuning. 18123–18133.
- Zhong, Z.; Cui, J.; Yang, Y.; Wu, X.; Qi, X.; Zhang, X.; and Jia, J. 2023. Understanding Imbalanced Semantic Segmentation Through Neural Collapse. *arXiv preprint arXiv:2301.01100*.
- Zhou, K.; Yang, J.; Loy, C. C.; and Liu, Z. 2022a. Conditional prompt learning for vision-language models. 16816–16825.
- Zhou, K.; Yang, J.; Loy, C. C.; and Liu, Z. 2022b. Learning to prompt for vision-language models. 1–12.
- Zhu, B.; Niu, Y.; Han, Y.; Wu, Y.; and Zhang, H. 2022. Prompt-aligned Gradient for Prompt Tuning. *arXiv preprint arXiv:2205.14865*.
- Zhu, Z.; Ding, T.; Zhou, J.; Li, X.; You, C.; Sulam, J.; and Qu, Q. 2021. A geometric analysis of neural collapse with unconstrained features. *Advances in Neural Information Processing Systems*, 34: 29820–29834.